

Received 23 October 2023, accepted 11 November 2023, date of publication 16 November 2023,
date of current version 21 November 2023.

Digital Object Identifier 10.1109/ACCESS.2023.3333692

RESEARCH ARTICLE

Bipartite Consensus of Fuzzy Multiagent Systems on Multilayer Cooperation Networks Using Output Measurements and Its Application to Image Communication

XINHUA WU¹, SUYING SHENG², AND GUOPING LU¹

¹School of Information Engineering, Jiangsu College of Engineering and Technology, Nantong, Jiangsu 226007, China

²School of Electrical Engineering, Nantong University, Nantong, Jiangsu 226019, China

Corresponding author: Suying Sheng (shensy@ntu.edu.cn)

This work was supported in part by the National Natural Science Foundation of China under Grant 62073180, in part by the Doctoral Research Startup Fund Project of Nantong University, and in part by the Science and Technology Project of Nantong City under Grant MSZ21023.

ABSTRACT This paper deals with the problem of bipartite consensus for Takagi-Sugeno fuzzy multiagent systems on multilayer cooperation-competition networks and its application to image communication. Fuzzy control laws are proposed by using relative output measurements between neighboring agents, where additive couplings are considered to show the different layered-interactions. Sufficient conditions for bipartite consensus of the multilayer networks with signed graphs are obtained by using the signed graph theory, Lyapunov stability theory and Takagi-Sugeno fuzzy systems theory. Then, coupled chaotic Lorenz systems over multilayer signed-networks are illustrated to show the effectiveness of the obtained results. Finally, a new multiagent image communication system is constructed based on the bipartite consensus of the fuzzy multilayer cooperation multiagent network, in which two agents in different layers for point-to-point communication use the output measurements from their own and neighboring agents as the synchronous encryption/decryption keystreams. The experimental results show that the proposed multiagent image communication system has excellent performance against some classical attacks.

INDEX TERMS Bipartite consensus, multilayer networks, signed graph, Takagi-Sugeno fuzzy multiagent systems, image secure communication.

I. INTRODUCTION

Recent years have seen great interest in coordination of multiagent systems due to its practical applications in a variety of areas, such as coordination of unmanned vehicles [1], power sharing in islanded microgrids [2], and formation control of multiple underactuated surface vessels [3]. As one of the critical issues on coordination of multiagent systems, consensus of multiagent systems concentrates on designing a control protocol to come to an agreement by means of the local information depending on network topology, and much

The associate editor coordinating the review of this manuscript and approving it for publication was Bing Li.

work has been reported (see [4], [5], [6], and the references therein).

It is worth noting that most results on consensus control are developed under the assumption of cooperative interactions among neighboring agents. In many real multiagent systems, however, some agents are cooperative, while others are competitive, such as the Euler-Lagrange systems with cooperative-competitive interactions [7]. The cooperation-competition networks can be modeled by a signed graph with both positive and negative edges, where positive and negative edges represent cooperative and competitive interactions, respectively. In the past decade, there have been intensive researches on bipartite consensus for

various multiagent systems under signed graphs, such as linear multiagent systems [8], [9], [10], [11], nonlinear multiagent systems with Lipschitz constraints [12], [13], [14], [15], nonlinear systems based on Takagi-Sugeno (T-S) fuzzy model [16]. In particular, in [15], synchronization problem is considered for multilayer reaction-diffusion neural networks with cooperative-competitive interactions modeled by a multilayer signed graph.

As stated in [17], multilayer networks are networks with different kinds of interactions, which incorporate multiple sub-networks. Compared with the research on the synchronization problem of multiagent systems under multilayer unsigned graphs [18], [19], [20], [21], [22], [23], there are fewer papers on the synchronization of multiagent systems under multilayer signed graphs [24], [25], [26]. The problems of bipartite synchronization under multilayer signed graphs have been studied in the leader-following framework for integer-order [24] and fractional-order [25], [26] multiagent systems with Lipschitz nonlinear dynamic, respectively.

The well-known T-S fuzzy model [27] is a convenient and flexible tool to handle complex nonlinear systems including nonlinear complex networks [28], [29], [30], [31] and nonlinear multiagent systems [32], [33], [34]. Nevertheless, there were few literature related to T-S fuzzy control for nonlinear complex networks with signed graphs [35] or multiagent systems with signed graphs [36]. In [35], the authors have investigated bipartite synchronization of T-S fuzzy complex networks with signed graphs via the combination of impulsive control and fast fixed-time control. In [36], the authors have studied the bipartite consensus problem for T-S fuzzy multiagent systems via a non-fragile state-coupling control protocol. Moreover, both [35] and [36] focus on some single-layer and signed networks. To the best of our knowledge, the problem of bipartite consensus for T-S fuzzy multiagent systems on multilayer cooperation networks have not yet been investigated.

The existing applications of consensus in multiagent systems on cooperative networks mainly focus on sensor networks [37], mobile robot formation control [38], microgrid [39], image secure communication [40], etc. However, there are still no reports on image secure communication based on bipartite consensus of multiagent systems on multilayer cooperation networks. With the promotion of multiagent systems and the deepening of information exchange, this is an issue that cannot be ignored and has application prospects.

Motivated by the above-mentioned discussion, this paper will deal with the problem of bipartite consensus for T-S fuzzy multiagent systems on multilayer cooperation networks. The main contributions can be summarized as follows.

- (1) A class of multilayer signed networks is established based on the T-S fuzzy model. The couplings between agents are additive and antagonistic in this paper, which is more general than [35] and [36].
- (2) In order to guarantee the bipartite consensus, fuzzy consensus control laws are proposed by using the

output measurements rather than states information from neighboring agents, which is more general.

- (3) Based on the proposed bipartite consensus results, a new multiagent image secure communication system is constructed to verify the validity and feasibility of the proposed theoretical method.

The rest of our paper is organized as follows: The problem formulation is introduced in Section II. The main results about bipartite consensus for T-S fuzzy multiagent systems on multilayer cooperation networks are addressed in Section III. Section IV demonstrates the theoretical results through a numerical simulation. The application of bipartite consensus in a new multiagent image communication system is considered to further demonstrate the feasibility of the proposed results. In Section V, we provide the final conclusion.

II. PROBLEM FORMULATION

Consider a class of T-S fuzzy multiagent systems composed of N agents as follows.

Plant Rule q : IF $\zeta_1(t)$ is \prod_{q1} and $\zeta_2(t)$ is $\prod_{q2} \dots$ and $\zeta_p(t)$ is \prod_{qp} , THEN

$$\begin{aligned} \dot{x}_i(t) &= A_q x_i(t) + u_i(t) \\ y_i(t) &= C_q x_i(t), \quad i = 1, 2, \dots, N, \end{aligned} \quad (1)$$

where $\zeta_b(t)$ and \prod_{qb} are the premise variable and the fuzzy set, $b = 1, 2, \dots, p$, $q = 1, 2, \dots, r$, r is the number of the rules. A_q and C_q are known matrices. $x_i(t) = [x_{i1}(t), x_{i2}(t), \dots, x_{i n_x}(t)]^T \in \mathbb{R}^{n_x}$ is the state variable of node i , $y_i(t) \in \mathbb{R}^{n_y}$ is the output measurement of node i , $u_i(t)$ is the control input.

According to the fuzzy inference method, the overall fuzzy model of the system (1) can be written in the following compact form:

$$\begin{aligned} \dot{x}_i(t) &= \sum_{q=1}^r \varpi_q(\zeta) A_q x_i(t) + u_i(t) \\ y_i(t) &= \sum_{q=1}^r \varpi_q(\zeta) C_q x_i(t), \quad i = 1, 2, \dots, N, \end{aligned} \quad (2)$$

where $\zeta = [\zeta_1, \zeta_2, \dots, \zeta_p]$, $\varpi_q(\zeta)$ is the normalized membership function defined by $\varpi_q(\zeta) = \frac{h_q(\zeta)}{\sum_{q=1}^r h_q(\zeta)}$, $h_q(\zeta) =$

$\prod_{b=1}^p \prod_{qb}(\zeta_b)$, where $\prod_{qb}(\zeta_b)$ represents the degree of the membership of ζ_b in \prod_{qb} . It is assumed that $h_q(\zeta) \geq 0$ and $\sum_{q=1}^r h_q(\zeta) > 0$. Then, it follows that $\varpi_q(\zeta) \geq 0$ and $\sum_{q=1}^r \varpi_q(\zeta) = 1$.

Due to the fact that there exist multiple interactions between agents and we do not always get available knowledge of the states, a distributed and output-measurements-based controller with M -layered antagonistic interactions is proposed as follows.

Controller Rule q : IF $\zeta_1(t)$ is \prod_{q1} and $\zeta_2(t)$ is \prod_{q2} ... and $\zeta_p(t)$ is \prod_{qp} , THEN

$$u_i(t) = H_q \sum_{k=1}^M \sum_{j=1}^N c^{(k)} |a_{ij}^{(k)}| \left(\text{sign}(a_{ij}^{(k)}) y_j(t) - y_i(t) \right) \quad (3)$$

where H_q indicates the gain matrix to be designed in order to achieve bipartite consensus, $c^{(k)}$ is the coupling strength, $\mathcal{A}^{(k)} = (a_{ij}^{(k)})_{N \times N}$ is the adjacency matrix of the k th layer, in which $a_{ij}^{(k)}$ is defined as follows. If there is a connection between agent i and agent j ($j \neq i$), then $a_{ij}^{(k)} = a_{ji}^{(k)} \neq 0$, otherwise, $a_{ij}^{(k)} = a_{ji}^{(k)} = 0$ ($j \neq i$). Specifically, if $a_{ij}^{(k)} = a_{ji}^{(k)} > 0$ (< 0), then the interaction between agent i and agent j is cooperative (competitive). $\text{sign}(\cdot)$ is defined as:

$$\text{sign}(\zeta) = \begin{cases} 1, & \zeta > 0 \\ 0, & \zeta = 0 \\ -1, & \zeta < 0 \end{cases}$$

Then, the defuzzified output of the fuzzy controller is given in the following form:

$$u_i(t) = \sum_{q=1}^r \varpi_q(\zeta) H_q \sum_{k=1}^M \sum_{j=1}^N c^{(k)} |a_{ij}^{(k)}| \left(\text{sign}(a_{ij}^{(k)}) y_j(t) - y_i(t) \right) \quad (4)$$

Remark 1: In this paper, the membership function is assumed to be available, hence the parallel distributed compensator (PDC) controller design is performed. In the PDC design, the fuzzy controller (3) shares the same membership functions (MFs) with the equation (2). There is an advantage in using the PDC control method: feedback gains can be combined with the MFs of the model during the closed-loop stability analysis, leading to genuine generalizations as they may relax the too-demanding requirement of a common feedback gain [41].

For each $k \in \{1, 2, \dots, M\}$, we denote $\mathcal{G}^{(k)} = (\mathcal{V}, \mathcal{E}^{(k)}, \mathcal{A}^{(k)})$, where $\mathcal{V} = \{1, 2, \dots, N\}$ and $\mathcal{E}^{(k)} \subseteq \mathcal{V} \times \mathcal{V}$. It is assumed that there is no self-loop in each layer.

For each layer $k \in \{1, 2, \dots, M\}$, the Laplace matrix of the signed graph $\mathcal{G}^{(k)}$ is defined as $\mathcal{L}^{(k)} = \mathcal{D}^{(k)} - \mathcal{A}^{(k)}$, where $\mathcal{D}^{(k)} = \text{diag}\{\sum_{j=1}^N |a_{1j}^{(k)}|, \dots, \sum_{j=1}^N |a_{Nj}^{(k)}|\}$. Let $\Gamma = \text{diag}\{\gamma_1, \dots, \gamma_N\}$, where $\gamma_i = 1$ for $i \in \mathcal{V}_1$ and $\gamma_i = -1$ for $i \in \mathcal{V}_2$.

Assumption 1: For each layer $k \in \{1, 2, \dots, M\}$, the signed graph $\mathcal{G}^{(k)}$ is connected.

Assumption 2: The multilayer and signed graphs $\mathcal{G}^{(k)}$, $k \in \{1, 2, \dots, M\}$ are structurally balanced, which means that there exists a bipartition of two nonempty node sets \mathcal{V}_1 and \mathcal{V}_2 with $\mathcal{V}_1 \cup \mathcal{V}_2 = \mathcal{V}$, $\mathcal{V}_1 \cap \mathcal{V}_2 = \emptyset$ such that $a_{ij}^{(k)} \geq 0$ if agent i and agent j belong to the same subset, otherwise $a_{ij}^{(k)} \leq 0$.

Remark 2: The structure of the controller is similar to the one in [42]. If $M = 1$, the signed graph $\mathcal{G}^{(k)}$ becomes the

single-layer signed graph. In the case of single-layer signed networks, Assumption 1 and Assumption 2 have usually been made to study bipartite consensus problems [7], [36], [43].

Definition 1 [44]: The bipartite consensus is achieved if the following condition is satisfied:

$$\lim_{t \rightarrow \infty} \left(x_i(t) - \frac{1}{N} \sum_{j=1}^N \gamma_i \gamma_j x_j(t) \right) = 0, \quad i = 1, 2, \dots, N.$$

Remark 3: The notion of bipartite consensus in Definition 1 means that all the agents in a network with cooperative-competitive interactions will finally achieve the bipartite average states of all agents. When all the interactions among agents over a multiagent network are cooperative, the notion of bipartite consensus in Definition 1 becomes the classical consensus [45]. In contrast to canonical consensus problems, such as the rendezvous control problem for networked nonholonomic mobile robots under the assumption that all the interactions among robots are cooperative [45], [46], this paper tries to solve bipartite consensus problem for T-S fuzzy multiagent systems from the multilayer and signed network point of view. The primary challenges include revealing the relationship among the multilayer and signed topologies, node dynamics in the T-S fuzzy form and the bipartite consensus, and facilitating the verification of the bipartite consensus condition.

III. MAIN RESULTS

For each agent $i \in \mathcal{V}$, define the bipartite consensus error $e_i(t) = x_i(t) - \frac{1}{N} \sum_{j=1}^N \gamma_i \gamma_j x_j(t)$. Then, by Assumption 1 and Assumption 2, it follows that

$$\begin{aligned} & \sum_{k=1}^M \sum_{j=1}^N c^{(k)} |a_{ij}^{(k)}| (\text{sign}(a_{ij}^{(k)}) x_j(t) - x_i(t)) \\ &= \sum_{k=1}^M \sum_{j=1}^N c^{(k)} |a_{ij}^{(k)}| (\text{sign}(a_{ij}^{(k)}) e_j(t) - e_i(t)). \end{aligned} \quad (5)$$

Therefore, the dynamic of the bipartite consensus error $e_i(t)$ is given as follows:

$$\begin{aligned} \dot{e}_i(t) &= \sum_{q=1}^r \sum_{\bar{q}=1}^r \varpi_q(\zeta) \varpi_{\bar{q}}(\zeta) [A_q e_i(t) \\ &+ H_{\bar{q}} C_q \sum_{k=1}^M \sum_{j=1}^N c^{(k)} |a_{ij}^{(k)}| (\text{sign}(a_{ij}^{(k)}) e_j(t) - e_i(t))]. \end{aligned} \quad (6)$$

Let $\bar{e}_i(t) = \gamma_i e_i(t)$, $\bar{e}(t) = [\bar{e}_1^T(t) \quad \bar{e}_2^T(t) \quad \dots \quad \bar{e}_N^T(t)]^T$. Then, it follows that

$$\begin{aligned} \dot{\bar{e}}(t) &= \sum_{q=1}^r \sum_{\bar{q}=1}^r \varpi_q(\zeta) \varpi_{\bar{q}}(\zeta) [(I_N \otimes A_q) \\ &- \sum_{k=1}^M c^{(k)} (W^{(k)} \otimes H_{\bar{q}} C_q)] \bar{e}(t), \end{aligned} \quad (7)$$

where $W^{(k)} = \Gamma \mathcal{L}^{(k)} \Gamma$.

Since the signed graph $\mathcal{G}^{(k)}$ ($k \in \{1, \dots, M\}$) is undirected and structurally balanced, matrix $W^{(k)}$ is real symmetric. Then, there exists an orthogonal matrix T such that

$$T^{-1}W^{(k)}T = \Lambda^{(k)}, \quad (8)$$

where $\Lambda^{(k)} = \text{diag}\{\lambda_1^{(k)}, \lambda_2^{(k)}, \dots, \lambda_N^{(k)}\}$, and $\lambda_i^{(k)}$ ($i = 1, 2, \dots, N$) are the eigenvalues of matrix $W^{(k)}$.

Let $\bar{e}(t) = (T \otimes I_{n_x})\hat{e}(t)$ and $\hat{e}(t) = [\hat{e}_1^T(t), \hat{e}_2^T(t), \dots, \hat{e}_N^T(t)]^T$, then,

$$\begin{aligned} \dot{\hat{e}}(t) &= \sum_{q=1}^r \sum_{\tilde{q}=1}^r \varpi_q(\zeta)\varpi_{\tilde{q}}(\zeta)[(I_N \otimes A_q) \\ &\quad - \sum_{k=1}^M c^{(k)}(\Lambda^{(k)} \otimes H_{\tilde{q}}C_q)]\hat{e}(t), \end{aligned} \quad (9)$$

which is equivalent to

$$\dot{\hat{e}}_i(t) = \sum_{q=1}^r \sum_{\tilde{q}=1}^r \varpi_q(\zeta)\varpi_{\tilde{q}}(\zeta)F_{i\tilde{q}q}\hat{e}(t), \quad i = 1, 2, \dots, N, \quad (10)$$

where $F_{i\tilde{q}q} = A_q - \sum_{k=1}^M c^{(k)}\lambda_i^{(k)}H_{\tilde{q}}C_q$.

It can be found that if $\lim_{t \rightarrow \infty} \|\hat{e}_i(t)\| = 0, i = 1, 2, \dots, N$, then $\lim_{t \rightarrow \infty} \|e_i(t)\| = 0, i = 1, 2, \dots, N$. Therefore, the problem of bipartite consensus for the fuzzy multilayer cooperation network (2) with the controller is transformed to the stability of N subsystems (10).

Theorem 1: The fuzzy multilayer cooperation network (2) achieves bipartite consensus under the controller (4) if there exist matrices $P > 0$ and $\hat{H}_q (q = 1, \dots, r)$ such that

$$\Omega_{i\tilde{q}q} < 0, \quad q = 1, \dots, r, \quad i = 1, \dots, N, \quad (11)$$

$$\Omega_{i\tilde{q}\tilde{q}} + \Omega_{i\tilde{q}q} < 0, \quad 1 \leq q < \tilde{q} \leq r, \quad i = 1, \dots, N, \quad (12)$$

where $\Omega_{i\tilde{q}\tilde{q}} = PA_q + A_q^T P - \sum_{k=1}^M c^{(k)}\lambda_i^{(k)}(\hat{H}_{\tilde{q}}C_q + C_q^T \hat{H}_{\tilde{q}}^T)$. In this case, the matrices $H_q (q = 1, \dots, r)$ can be obtained as

$$H_q = P^{-1}\hat{H}_q, \quad q = 1, \dots, r. \quad (13)$$

Proof: In order to demonstrate that the bipartite consensus is achieved, it is enough to show N subsystems (10) are asymptotically stable. Choose the Lyapunov function for the system (10) as

$$V_i(t) = \hat{e}_i^T(t)P\hat{e}_i(t), \quad (14)$$

Then, along the trajectories of the system (10), the derivative of $V_i(t)$ yields

$$\begin{aligned} \dot{V}_i(t) &= 2\hat{e}_i^T(t)P\dot{\hat{e}}_i(t) \\ &= \hat{e}_i^T(t) \left[\sum_{q=1}^r \sum_{\tilde{q}=1}^r \varpi_q(\zeta)\varpi_{\tilde{q}}(\zeta) \left(PF_{i\tilde{q}\tilde{q}} + F_{i\tilde{q}q}^T P \right) \right] \hat{e}_i(t) \end{aligned}$$

$$= \hat{e}_i^T(t) \left[\sum_{q=1}^r \sum_{\tilde{q}=1}^r \varpi_q(\zeta)\varpi_{\tilde{q}}(\zeta)\Phi_{i\tilde{q}\tilde{q}} \right] \hat{e}_i(t), \quad (15)$$

where $\Phi_{i\tilde{q}\tilde{q}} = PA_q + A_q^T P - \sum_{k=1}^M c^{(k)}\lambda_i^{(k)}(PH_{\tilde{q}}C_q + C_q^T H_{\tilde{q}}^T P)$.

Let $PH_q = \hat{H}_q, q = 1, \dots, r$, then $H_q = P^{-1}\hat{H}_q, q = 1, \dots, r$, and $\Phi_{i\tilde{q}\tilde{q}}$ becomes $\Omega_{i\tilde{q}\tilde{q}}$. It follows from (11) and (12) that $\dot{V}_i(t) < 0$ for $\hat{e}_i(t) \neq 0$. Therefore, N subsystems (10) are asymptotically stable. This completes the proof.

Remark 4: Theorem 1 indicates that the criterion of bipartite consensus for T-S fuzzy multiagent systems over multilayer and signed networks is equivalent to the stability condition of N subsystems (10). This decoupled result is based on the assumption that the multilayer and signed graphs are undirected. It is a limitation of the proposed consensus algorithm.

Remark 5: The decoupled result given by Theorem 1 can be applied to solve the bipartite consensus problem of T-S fuzzy multiagent systems over multilayer networks with a large number of agents. This is an advantage of the proposed bipartite consensus strategy. Meanwhile, there also exist some disadvantages. First, the multilayer and signed graphs are required to be undirected and structurally balanced, and this may result in limitations of the proposed method in practice. Second, the proposed method does not consider the communication delay. These will be our research topic in near future.

IV. NUMERICAL EXAMPLE

Consider the fuzzy multilayer cooperation network (2) with 6 agents and 2 layers, where the multilayer cooperation network topology is shown in Fig. 1, where both Layer 1 and Layer 2 are structurally balanced with the bipartition of the nodes $\mathcal{V}_1 = \{1, 2, 3\}$ and $\mathcal{V}_2 = \{4, 5, 6\}$, which satisfies Assumption 2.

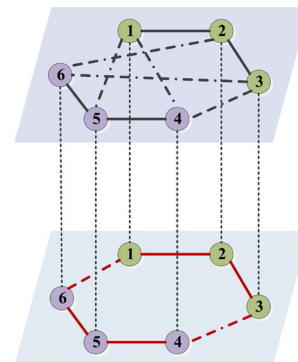


FIGURE 1. Two-layer competition networks with six nodes.

The T-S fuzzy chaotic Lorenz system is considered as each agent, and the parameters are given as follows:

$$A_1 = \begin{bmatrix} -10 & 10 & 0 \\ 28 & -1 & 25 \\ 0 & -25 & -8/3 \end{bmatrix},$$

$$A_2 = \begin{bmatrix} -10 & 10 & 0 \\ 28 & -1 & -25 \\ 0 & 25 & -8/3 \end{bmatrix},$$

$$C_1 = \begin{bmatrix} 1 & 1 & 0 \\ 0 & 1 & 1 \end{bmatrix}, \quad C_2 = \begin{bmatrix} 0 & 1 & 0 \\ 0 & 0 & 1 \end{bmatrix},$$

Suppose that $c^{(1)} = 0.1$, $c^{(2)} = 1$. Then by solving the linear matrix inequalities (11) and (12) in Theorem 1, the controller gain matrices are obtained as follows:

$$H_1 = \begin{bmatrix} 8.9743 & 5.5396 \\ 29.9682 & 6.9860 \\ 21.6075 & 27.2358 \end{bmatrix},$$

$$H_2 = \begin{bmatrix} 17.2925 & 5.5743 \\ 40.7321 & 6.0500 \\ 0.9494 & 27.6925 \end{bmatrix}.$$

In the simulation, by using the sector nonlinearity approach [47], the membership functions are taken as $\varpi_1(x_{11}(t)) = \frac{-x_{11}(t)+25}{50}$, $\varpi_2(x_{11}(t)) = 1 - \varpi_1(x_{11}(t))$. Fig. 2 exhibits a chaotic behavior of agent 1 in the absence of controller. Fig. 3 represents the state trajectories of the agents with the designed controllers. Fig. 4 shows the evolution of the bipartite consensus errors, from which it can be found that the bipartite consensus is achieved.

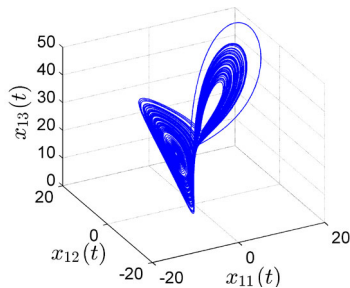


FIGURE 2. Chaotic behavior of agent 1 without controller.

V. APPLICATION OF BIPARTITE CONSENSUS TO IMAGE COMMUNICATION

In this section, a multiagent image communication system is constructed to verify the validity and practicality of the obtained results in section II and III. Meanwhile the proposed bipartite consensus results are the key to the implementation of the multiagent image communication system.

A. SYSTEM DESCRIPTION

In the practical applications of multiagent systems, such as the coordination of unmanned vehicles, power sharing in islanded microgrids, and formation control of multiple underactuated surface vessels, information exchange and sharing are all involved. However, in the process of network information transmission, security issues such as network eavesdropping and deception attacks may be encountered, so it is necessary to encrypt the transmitted information.

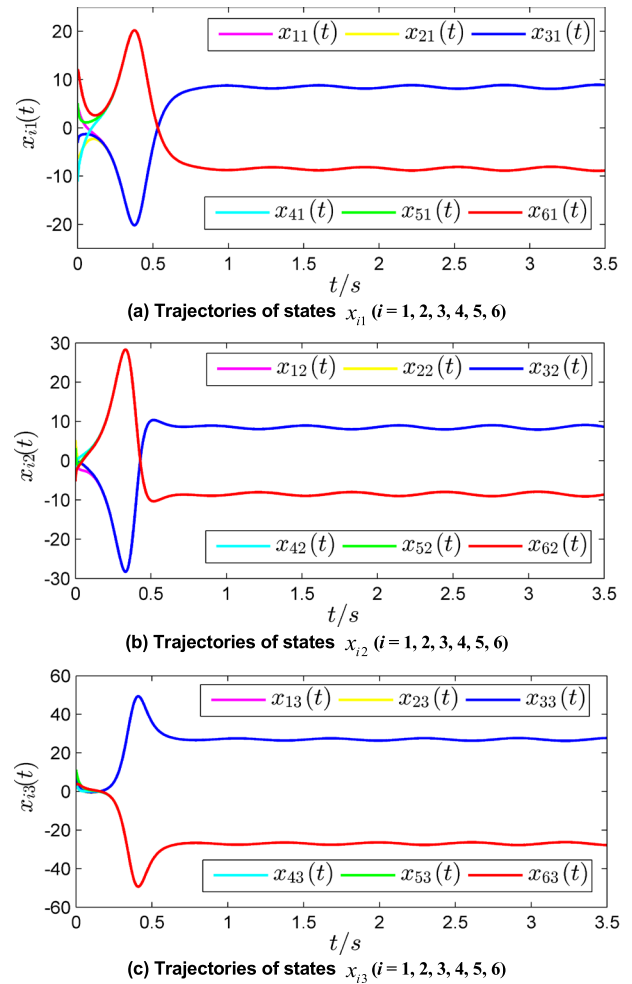


FIGURE 3. Trajectories of states x_{i1} , x_{i2} and x_{i3} with the controller.

In this case, a multiagent image secure communication system is proposed and constructed based on the bipartite consensus.

For a fuzzy multiagent system on a multilayer cooperation network, it is assumed that each agent is equipped with an image encryption/decryption device which has no impact on the dynamic model of the agent itself. The typical multiagent image communication system consists of two parts, namely the transmitter and receiver, as shown in Fig. 5. Without loss of generality, take the example of multiagent image secure communication in different network layers, such as transmitting color or grayscale images from agent i in the upper layer to agent j in the lower layer.

Using the output measurements of its own and neighboring agents as the encryption keystreams, the agent i encrypts the plain image. The specific encryption algorithm is shown in section V-B. Subsequently, the encrypted image, the characteristic information of the plain image and the transmitted agent number i are combined into a data packet for transmission. After receiving the data packet, the agent j splits the data packet, and similarly uses the output measurements from

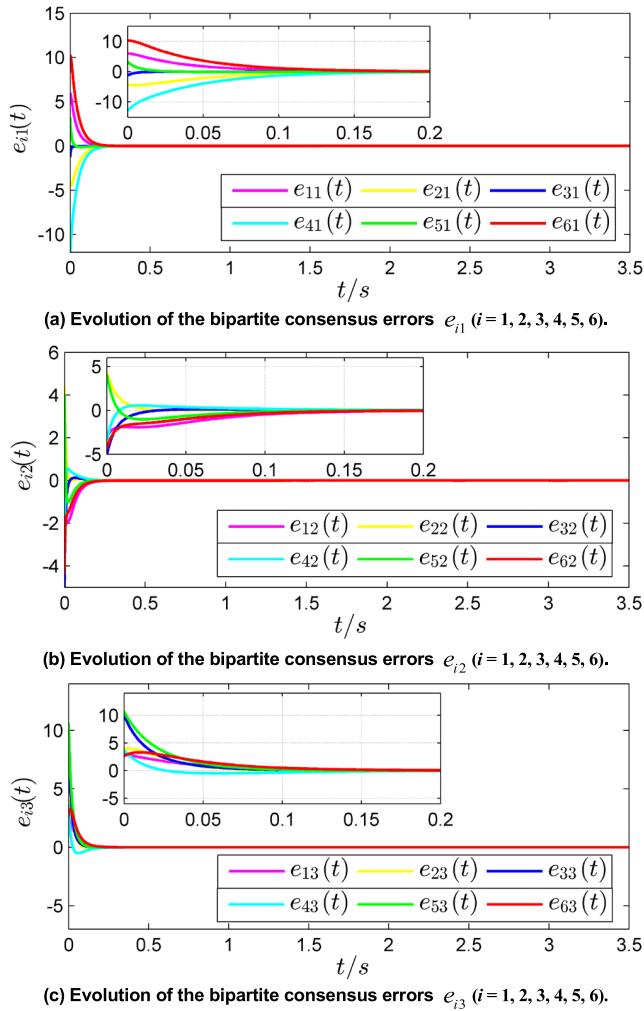


FIGURE 4. Evolution of all bipartite consensus errors.

its own and neighboring agents as the decryption keystreams to decrypt the decomposed image. The specific decryption algorithm is shown in section V-B. It is worth mentioning that the channel for packet transmission is independent of the multiagent signed network, and the transmission adopts “one image, one packet, single transmission” mode.

Image encryption/decryption keystreams come from output measurements generated by its own agent and adjacent agents with connection. However, how can we ensure that the encryption and decryption keystreams are synchronized? With the proposed fuzzy consensus control laws, the bipartite consensus for T-S fuzzy multiagent systems on multilayer cooperation networks can be achieved, that is, the output measurements of all agents can also achieve bipartite consensus.

Remark 6: The output measurements from the agent itself and its neighboring agents are used as encryption and decryption keystreams, which is different from the states information from neighboring agents as keystreams. To the best of our knowledge, for a signed network with balanced structure, any agent has at least one neighboring agent. Using

output measurements as keystreams for parallel encryption/ decryption can not only facilitate applications, but also improve encryption efficiency.

Remark 7: The idea of internal keys is introduced, where the characteristic information of plain image is used as the internal keys for image encryption. Only when the image encryption keys and decryption keys are completely consistent, including the internal keys and external keys, can the effective operation of multiagent image secure communication system be guaranteed, as well as the recovery of the original plain image.

B. IMAGE ENCRYPTION/DECRYPTION ALGORITHM

The proposed image encryption/decryption algorithm adopts a framework of “permutation-diffusion”, which utilizes relative output measurements as keystreams for image encryption/ decryption based on bipartite consensus. Simultaneously considering the combination of external and internal keys, the image encryption and decryption results not only rely on external keys and keystreams, but also depend on the original plain image.

Without losing generality, the proposed algorithm is applied to both color and grayscale images, and the specific algorithm steps are described as follows.

Step 1: Layer the plain image A as shown in Fig. 6 to obtain 8 bit-level images, represented as $BL_1, BL_2, BL_3, BL_4, BL_5, BL_6, BL_7, BL_8$.

At the same time, we establish the characteristic information ξ_A of the plain image, which is the internal key for image encryption, calculated as follows:

$$\xi_A = \frac{\sum_{k=1}^m \sum_{l=1}^L (1 + 0.17 \times k + 0.37 \times l)P(k, l)}{300 \times 256 \times m \times L}$$

where $L = 3n$ for color image and $L = n$ for grayscale image.

Step 2: Layer extraction - Circular bit-shifting (row by row, column by column) - Layer backfilling

(1) Extract the 1st, 3rd, 5th, 7th, 9th, 11th, 13th and 15th decimal values of characteristic information ξ_A using a customized function $\eta(\xi_A, k) = \lfloor (\xi_A \times 10^{k-1} - \lfloor \xi_A \times 10^{k-1} \rfloor) \times 10 \rfloor$, and obtain the sequence $S = \{\eta(\xi_A, 1), \eta(\xi_A, 3), \eta(\xi_A, 5), \eta(\xi_A, 7), \eta(\xi_A, 9), \eta(\xi_A, 11), \eta(\xi_A, 13), \eta(\xi_A, 15)\}$.

According to the ascending sorting rule of sequence S , certain layers are extracted from the 8 layer bit-level images in order, and the extracted layers are concatenated up and down to form a matrix BP , with a size of $8m \times 3n$ or $8m \times n$.

(2) For the setting external encryption key R_Sft , we perform a circular right bit-shifting operation on the matrix BP row by row, where the number of bit-shifts in the k th row is expressed as follows,

$$\text{Number_Sft1} = \text{mod} \left(\left\lfloor y_i(1, R_Sft) \times 10^{12} + \xi_A \times 10^{13} \right\rfloor, L \right) \quad (16)$$

where $y_i(1, R_Sft)$ is the output measurement of agent i at time R_Sft . At the same time, after each row shift, update the

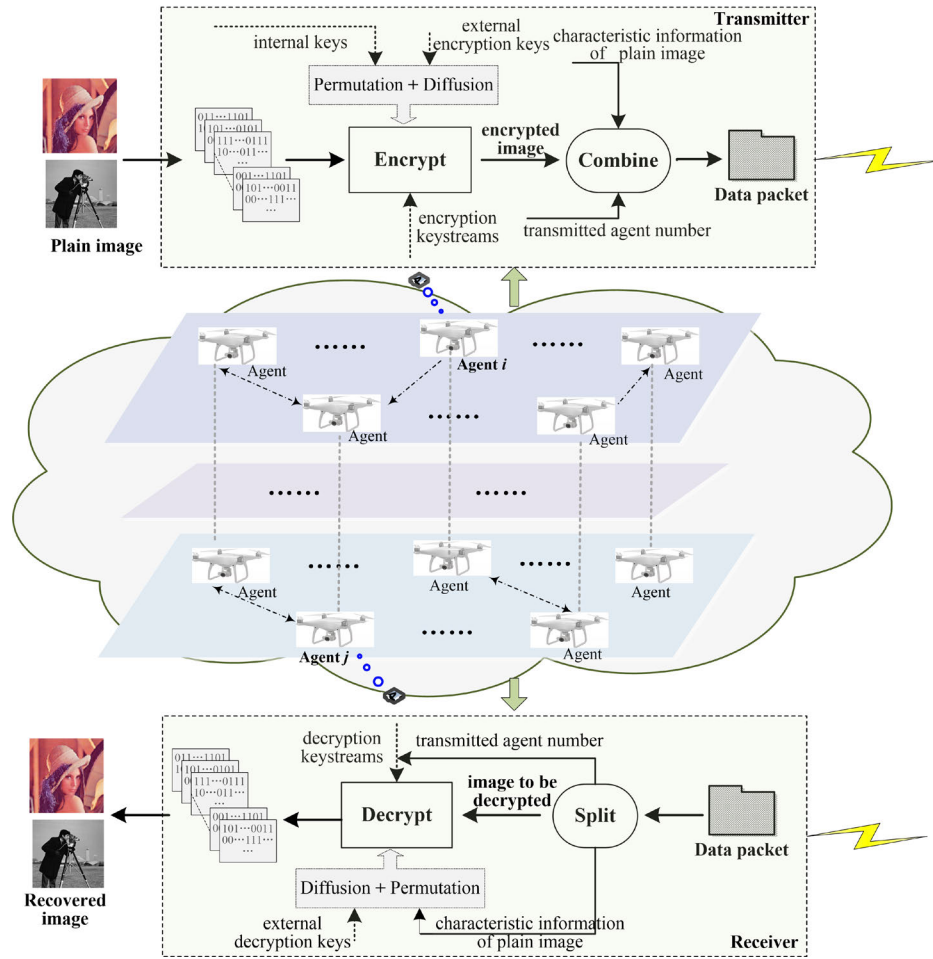


FIGURE 5. Block diagram of the multiagent image communication system based on bipartite consensus.

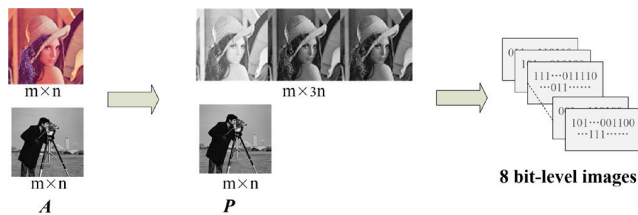


FIGURE 6. Image layer process.

external key R_{Sft} , which is

$$R_{Sft} = R_{Sft} + \text{bin2dec}(BP(k, L - 8 : L - 5)) + 1.$$

Repeat the above process until the last row.

Then for the setting external encryption key C_{Sft} , we perform a circular upward bit-shifting operation on the matrix BP column by column, where the number of bit-shifts in the l th column is calculated as follows,

$$\begin{aligned} & \text{Number_Sft2} \\ & = \text{mod} \left(\lfloor y'_i(2, C_{Sft}) \times 10^{14} + \xi_A \times 10^{15} \rfloor, 8m \right) \quad (17) \end{aligned}$$

where $y'_i(2, C_{Sft})$ is the output measurement from a neighboring agent of agent i at time C_{Sft} . At the same time, after each column shift, update the external key P_{Sft} as

$$C_{Sft} = C_{Sft} + \text{bin2dec}(BP(8m - 8 : 8m - 5, l)) + 1.$$

Repeat the above process until the last column.

(3) Similarly, using the customized function $\eta(\xi_A, k)$, extract the 2nd, 4th, 6th, 8th, 10th, 12th, 14th and 16th decimal values of characteristic information ξ_A to obtain the sequence $S = \{\eta(\xi_A, 1), \eta(\xi_A, 3), \eta(\xi_A, 5), \eta(\xi_A, 7), \eta(\xi_A, 9), \eta(\xi_A, 11), \eta(\xi_A, 13), \eta(\xi_A, 15)\}$. According to the descending sorting rule of sequence S , the matrix BP is evenly divided into 8 blocks from top to bottom, and backfilled into the 8 layer bit-level images to obtain the permuted numerical matrix PC .

Remark 8: The proposed ‘‘permutation’’ operation of the proposed image encryption algorithm embeds row and column cyclic bit-shifting into the layer extraction and backfilling of 8 bit-level images, which is different from the common pixel scrambling and layered bit-level image shifting directly. By combining the layer extraction and backfilling relying on internal keys with the cyclic bit-shifting relying on

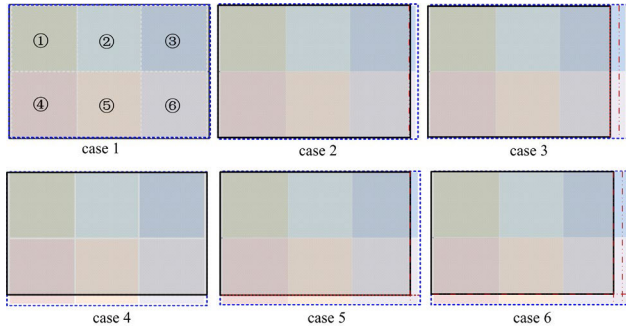


FIGURE 7. Cases of different partition blocks.

external keys, the algorithm has both confusion and diffusion functions.

Step 3: Set the external encryption keys S_dif , E_dif and V_dif , and divide the image matrix PC into 6 blocks as shown in the Fig. 7, where the actual size is indicated by a solid black line, while the ideal size that can be divided equally is indicated by a dashed blue line. These 6 image blocks can undergo parallel diffusion operations simultaneously. As shown in the figure, there may be situations where the image matrix PC cannot be evenly divided (such as labeled cases 2-6). Please refer to Algorithm 1 for details.

Remark 9: The “diffusion” operation of the proposed image encryption algorithm takes only dividing the image into 6 blocks as an example for parallel diffusion. In fact, due to the diversity of the combination methods of the output measurements of the agent itself and its neighboring agents, the image can be divided into more blocks, which can greatly improve the efficiency of image encryption.

Step 4: According to the layering method in step 1, reorganize the diffused image C to obtain the encrypted image.

Correspondingly, the image decryption algorithm is the inverse process of image encryption. It must be pointed out that whether the receiving agent can perfectly recover the original plain image depends on three aspects. Firstly, the multiagent system can achieve bipartite consensus to ensure that the encryption and decryption keystreams are bipartite synchronized accordingly. Secondly, the internal encryption key is packaged and sent by the data packet, ensuring the consistency of the internal key at the receiving and sending ends. Finally, the external encryption keys and external decryption keys must be exactly the same, which can be agreed upon in advance.

C. EXPERIMENT AND PERFORMANCE ANALYSIS

Based on the example in Section IV, the network topology and system parameters of the multilayer multiagent system have been given. Assuming that in the multiagent communication system, agent 3 on the upper layer transmits images to agent 5 on the lower layer. The output measurements of agent 3 and its neighboring agents (such as 2, 4, 6) are used as the encryption keystreams, while the output measurements

Algorithm 1 Image Diffusion Encryption Step

```

Set the external encryption keys  $S\_dif$ ,  $E\_dif$  and  $V\_dif$ ,
the transient values  $Y_{1\_tmp}$ ,  $Y_{2\_tmp}$ ,  $Y_{3\_tmp}$ ,  $Y_{4\_tmp}$ ,
 $Y_{5\_tmp}$  and  $Y_{6\_tmp}$ ;
 $[L_1, L_2]=size(PC)$ ;
for  $k = 1:ceil(L_1/2)$ 
for  $l = 1:ceil(L_2/3)$ 
 $Y_1 = \text{mod}(\text{floor}(y_i(1, S\_dif)*10^{(\text{mod}(E\_dif,15)+1)}), 256)$ ;
 $Y_2 = \text{mod}(\text{floor}(y_i(2, S\_dif)*10^{(\text{mod}(E\_dif,15)+1)}), 256)$ ;
 $Y_3 = \text{mod}(\text{floor}(y_i(1, S\_dif) + y_i(2, S\_dif))$ 
 $*10^{(\text{mod}(E\_dif,15)+1)}, 256)$ ;
 $Y_4 = \text{mod}(\text{floor}((y'_i(1, S\_dif) - y'_i(2, S\_dif))$ 
 $*10^{(\text{mod}(E\_dif,15)+1)}, 256)$ ;
 $Y_5 = \text{mod}(\text{floor}((-y'_i(1, S\_dif) + y'_i(2, S\_dif))$ 
 $*10^{(\text{mod}(E\_dif,15)+1)}, 256)$ ;
 $Y_6 = \text{mod}(\text{floor}((-y'_i(1, S\_dif) - y'_i(2, S\_dif))$ 
 $*10^{(\text{mod}(E\_dif,15)+1)}, 256)$ ;
 $C(k, l) = \text{mod}(PC(k, l) + Y_1 - \text{bitxor}(V\_dif, Y_{1\_tmp}),$ 
 $256)$ ;
 $V\_dif = \text{mod}(V\_dif + C(k, l), 256)$ ; % block ①
 $C(k, ceil(L_2/3) + l) = \text{mod}(PC(k, ceil(L_2/3) + l) + Y_2 -$ 
 $\text{bitxor}(V\_dif, Y_{2\_tmp}), 256)$ ;
 $V\_dif = \text{mod}(V\_dif + C(k, ceil(L_2/3) + l), 256)$ ; % block ②
if  $l \leq (L_2 - 2 * ceil(L_2/3))$ 
 $C(k, 2 * ceil(L_2/3) + l) = \text{mod}(PC(k, 2 * ceil(L_2/3) + l) +$ 
 $Y_3 -$ 
 $\text{bitxor}(V\_dif, Y_{3\_tmp}), 256)$ ;
 $V\_dif = \text{mod}(V\_dif + C(k, 2 * ceil(L_2/3) + l), 256)$ ;
end % block ③
if  $k \leq (L_1 - ceil(L_1/2))$ 
 $C(ceil(L_1/2) + k, l) = \text{mod}(PC(ceil(L_1/2) + k, l) + Y_4 -$ 
 $\text{bitxor}(V\_dif, Y_{4\_tmp}), 256)$ ;
 $V\_dif = \text{mod}(V\_dif + C(ceil(L_1/2) + k, l), 256)$ ;
 $C(ceil(L_1/2) + k, ceil(L_2/3) + l) = \text{mod}(PC(ceil(L_1/2) + k,$ 
 $ceil(L_2/3) + l) + Y_5 - \text{bitxor}(V\_dif, Y_{5\_tmp}), 256)$ ;
 $V\_dif = \text{mod}(V\_dif + C(ceil(L_1/2) + k, ceil(L_2/3) + l), 256)$ ;
end % block ④,⑤
if  $k \leq (L_1 - ceil(L_1/2)) \&\& l \leq (L_2 - 2 * ceil(L_2/3))$ 
 $C(ceil(L_1/2) + k, 2 * ceil(L_2/3) + l) =$ 
 $\text{mod}(PC(ceil(L_1/2) + k,$ 
 $2 * ceil(L_2/3) + l) + Y_6 - \text{bitxor}(V\_dif, Y_{6\_tmp}), 256$ 
 $)$ ;
 $V\_dif = \text{mod}(V\_dif + C(ceil(L_1/2) + k, 2 * ceil(L_2/3) + l),$ 
 $256)$ ;
end % block ⑥
 $S\_dif = S\_dif + \text{mod}(V\_dif, 17) + 1$ ;
 $E\_dif = E\_dif + C(k, l) + C(k, ceil(L_2/3) + l) + V\_dif$ ;
 $Y_{1\_tmp} = Y_1$ ;  $Y_{2\_tmp} = Y_2$ ;  $Y_{3\_tmp} = Y_3$ ;
 $Y_{4\_tmp} = Y_4$ ;  $Y_{5\_tmp} = Y_5$ ;  $Y_{6\_tmp} = Y_6$ ;
end
end

```

of agent 5 and its neighboring agents (such as 4, 6) are used as the decryption keystreams.

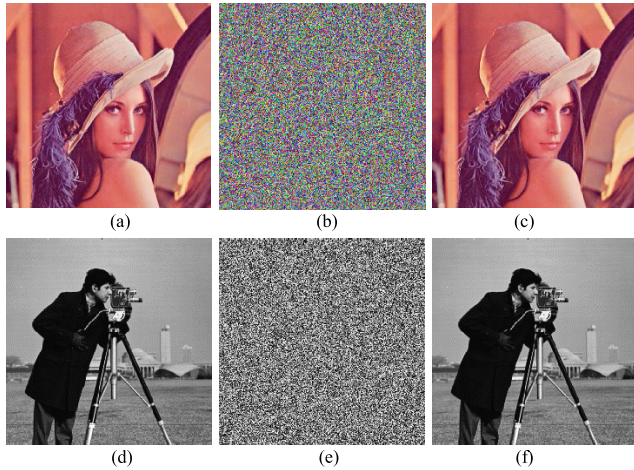


FIGURE 8. Encryption and decryption results of different images: (a) plain image, (b) encrypted image and (c) decrypted image of “Lena”; (d) plain image, (e) encrypted image and (f) decrypted image of “Cameraman”.

Given the external encryption keys as start shifting timestamps $R_Sft = 2234$ and $C_Sft = 2134$, start diffusion timestamp $S_dif = 2345$, diffusion initial value $V_dif = 98$, and diffusion exponential value $E_dif = 12$, the plain images “Lena” and “Cameraman” are encrypted by agent 3 respectively to obtain encrypted images. Then the encrypted image, characteristic value of the plain image, the number 3 of the transmitted agent are combined to form a data packet for transmission. Similarly, given the external decryption keys as start shifting timestamps $Rd_Sft = 2234$ and $Cd_Sft = 2134$, start diffusion timestamp $Sd_dif = 2345$, diffusion initial value $Vd_dif = 98$, and diffusion exponential value $Ed_dif = 12$, the agent 5 decrypts the encrypted image decomposed from the receiving data packet to obtain the decrypted image and recover the original plain image. The encryption and decryption results of color and grayscale images are shown in Fig. 8.

1) KEY SPACE

The encryption keys of the proposed image encryption scheme consist of encryption keystreams, internal encryption key and external encryption keys. The encryption keystreams are mainly related to the system model parameters (A_1, A_2, C_1 and C_2) and discretization step size T , the internal encryption key only depends on the original plain image, and the external encryption keys are discussed and set by the receiver and sender in advance, such as $R_Sft, C_Sft, S_dif, V_dif$ and E_dif . According to the computer’s calculation precision of 10^{-16} , the key space of the proposed image encryption scheme can amount to $10^{(16 \times 7 + 3 \times 5)} = 10^{127}$, which is large enough to resist exhaustive attacks.

2) KEY SENSITIVITY

A robust image secure communication must be sensitive to keys, that is, even a slight change of the keys can result in the “completely different” outcome. The key sensitivity of the

system is mainly analyzed from two aspects, the sensitivity of the encryption keys and the sensitivity of the decryption keys.

a: SENSITIVITY OF ENCRYPTION KEYS

To facilitate testing the sensitivity of encryption keys, only a single minor change is made to individual encryption key every time, such as $a = 10 + 10^{-15}$ or $b = 25 + 10^{-15}$ or $V_dif = 99$, so as to observe the difference of encrypted images. Comparing the encrypted image obtained from the slightly changed encryption keys with the encrypted image shown in Fig. 8 (b) and (e), the corresponding error images can be obtained, as shown in Fig. 9, where Fig. 9 (a) - (c) are the corresponding error images of color image “Lena”, and Fig. 9(d) - (f) are the corresponding error images of grayscale image “Cameraman”. Obviously, even a small change in the encryption keys can lead to significant differences between encrypted images.

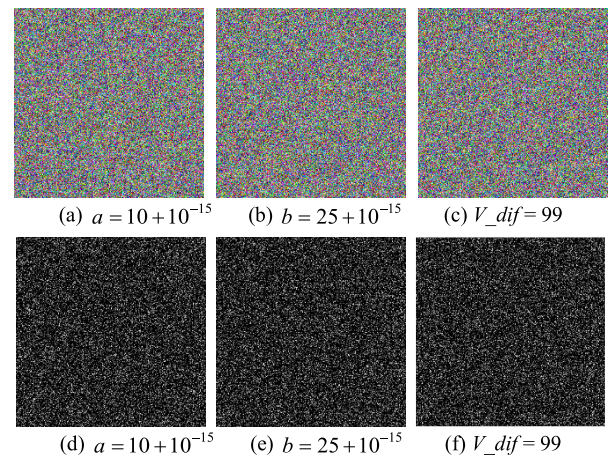


FIGURE 9. Error images with slight changed encryption keys, (a) - (c) are the corresponding error images of color image “Lena”, and (d) - (f) are the corresponding error images of grayscale image “Cameraman”.

In order to further quantitatively analyse the impact of subtle changes in encryption keys on encryption performance, NPCR (number of pixel change rates) and UACI (unified average change intensity) are introduced, as defined,

$$NPCR = \frac{\sum_{i=1}^m \sum_{j=1}^n D(i,j)}{m \times n} \times 100\% \tag{18}$$

$$UACI = \frac{\sum_{i=1}^m \sum_{j=1}^n |C_1(i,j) - C_2(i,j)|}{255 \times m \times n} \times 100\% \tag{19}$$

where $D(i,j)$ stands for the difference between encrypted image $C_1(i,j)$ and encrypted image $C_2(i,j)$, defined by the following formula,

$$D(i,j) = \begin{cases} 1, & \text{if } C_1(i,j) \neq C_2(i,j) \\ 0, & \text{else} \end{cases} \tag{20}$$

Here, we analyse the encryption effect of six types of slight changes in encryption keys, such as (1) $a = 10 + 10^{-15}$, (2) $b = 25 + 10^{-15}$, (3) $c = 28 + 10^{-15}$, (4) $R_Sft = 2235$,

TABLE 1. NPCR and UACI values of different images.

key change	NPCR			UACI		
	Red	Green	Blue	Red	Green	Blue
(1)	99.61%	99.61%	99.62%	33.41%	33.49%	33.44%
(2)	99.61%	99.55%	99.62%	33.38%	33.39%	33.43%
(3)	99.61%	99.60%	99.62%	33.49%	33.38%	33.34%
(4)	99.59%	99.55%	99.59%	33.51%	33.35%	33.36%
(5)	99.60%	99.60%	99.61%	33.60%	33.45%	33.43%
(6)	99.62%	99.60%	99.59%	33.43%	33.48%	33.39%

key change	NPCR	UACI
	Grayscale Pixel	Grayscale Pixel
(1)	99.60%	33.61%
(2)	99.59%	33.49%
(3)	99.61%	33.50%
(4)	99.59%	33.44%
(5)	99.58%	33.55%
(6)	99.65%	33.58%

(5) $C_Sft = 2344$ and (6) $V_dif = 99$, still using color image “Lena” and grayscale image “Cameraman” as examples. As shown in Table 1, the NPCR of the encrypted image is close to 1, and its UACI also reaches the ideal value, indicating that even a single slight change in the encryption key can lead to completely different encrypted image.

b: SENSITIVITY OF DECRYPTION KEYS

Similarly, only a single minor change is made to decryption keys each time, such as $\tilde{a} = 10 + 10^{-15}$ or $\tilde{b} = 25 + 10^{-15}$ or $Vd_dif = 99$. The decrypted effects of the color encrypted image (as shown in Fig. 8(b)) and the grayscale encrypted image (as shown in Fig. 8(e)) are exhibited in Fig. 10, respectively. As can be clearly seen, the recovered images are all in a mess and do not reveal any traces of plain images.

In order to assess the quality of decrypted images more clearly, PSNR (peak signal-to-noise ratio) and RMSE (root mean square error) are used to measure the difference between the decrypted image and original plain image. The PSNR is defined as,

$$PSNR = 10 \log_{10} \frac{255^2}{MSE} \tag{21}$$

where MSE (mean square error) is expressed as follows,

$$\left\{ \begin{aligned} MSE &= \frac{\sum_{i=1}^m \sum_{j=1}^n \sum_{k=1}^3 [X(i, j, k) - Y(i, j, k)]^2}{3 \times m \times n} \\ &\quad \text{for color image} \\ MSE &= \frac{\sum_{i=1}^m \sum_{j=1}^n [X(i, j) - Y(i, j)]^2}{m \times n} \\ &\quad \text{for gray scale image} \end{aligned} \right. \tag{22}$$

where m and n denote the size of the original image X and the compared image Y .

The RMSE is written as,

$$\left\{ \begin{aligned} RMSE &= \sqrt{\frac{\sum_{i=1}^m \sum_{j=1}^n \sum_{k=1}^3 [X(i, j, k) - Y(i, j, k)]^2}{3 \times m \times n}} \\ &\quad \text{for color image} \\ RMSE &= \sqrt{\frac{\sum_{i=1}^m \sum_{j=1}^n [X(i, j) - Y(i, j)]^2}{m \times n}} \\ &\quad \text{for gray scale image} \end{aligned} \right. \tag{23}$$

The PSNR and RMSE of decrypted images in Fig.8 (c) and (f) are ∞ and 0, respectively, which is an ideal condition to prove that the decrypted images have the same values as plain images. The adopted subtle changes in decryption keys are similar to encryption keys. However, the PSNR and RMSE values of the decrypted images are completely different from the ideal values, as shown in Table 2.

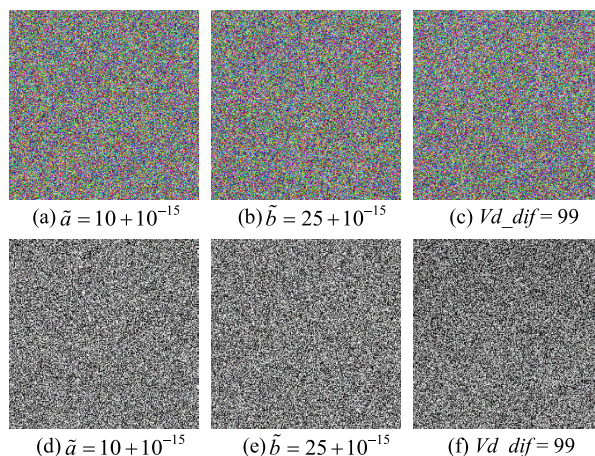


FIGURE 10. Decrypted images with slight changed decryption keys (a-c for color image “Lena”, d-f for gray image “Cameraman”).


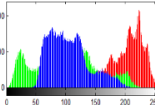

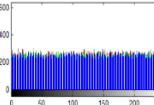

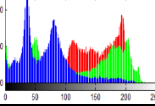

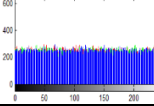

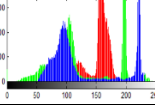
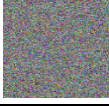
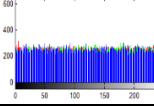

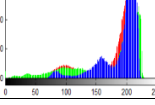
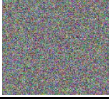
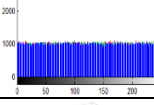

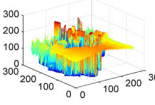
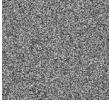
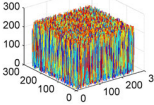

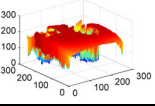

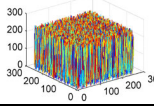

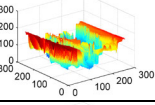
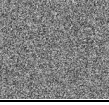
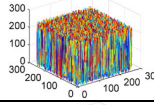

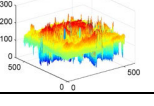

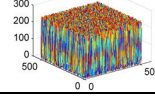
TABLE 2. NPCR and UACI values of different images.

key change	Plain image	RMSE	PSNR	Plain image	RMSE	PSNR
no change		0	∞		0	∞
(1)		94.5137	8.6209		96.8407	8.4096
(2)		94.2815	8.6423		96.9714	8.3979
(3)		94.5522	8.6174		96.9027	8.4041
(4)		93.9777	8.6703		95.9491	8.4900
(5)		94.6288	8.6103		97.4644	8.3539
(6)		94.3548	8.6355		97.1570	8.3813

3) PERFORMANCE AGAINST STATISTICAL ATTACKS

Statistical attacks are used to decipher original image information by analyzing the statistical rules of encrypted images, which are mainly reflected in the histogram, correlation and information entropy of the image. That is to say, an excellent image encryption scheme must be able to resist statistical

TABLE 3. Histograms of several images.

	Plain image	Histogram	Encrypted image	Histogram
1				
2				
3				
4				
5				
6				
7				
8				

attacks including histogram, correlation, and information entropy of the image.

a: HISTOGRAM

Some typical images are selected from the standard image database, which have been tested and presented in Table 3, including four color images (“Lena”, “Peppers”, “House”, “Airplane”) and four grayscale images (“Cameraman”, “Clock”, “Pallon”, “Boat”). From Table 3, it can be demonstrated that the histograms displayed in the last column is completely different from the histograms shown in the third column, with uniform distribution to eliminate the distribution information of the original plain image.

b: CORRELATION

To analyze the correlation performance, 10000 pairs of adjacent pixels (horizontal, vertical, diagonal, and counter-diagonal directions) are randomly selected from plain and encrypted images. Still taking the color image “Lena” and grayscale image “Cameraman” as examples, Fig. 11 exhibits the correlation distribution between different color channels and different adjacent pixel directions, which indicates that

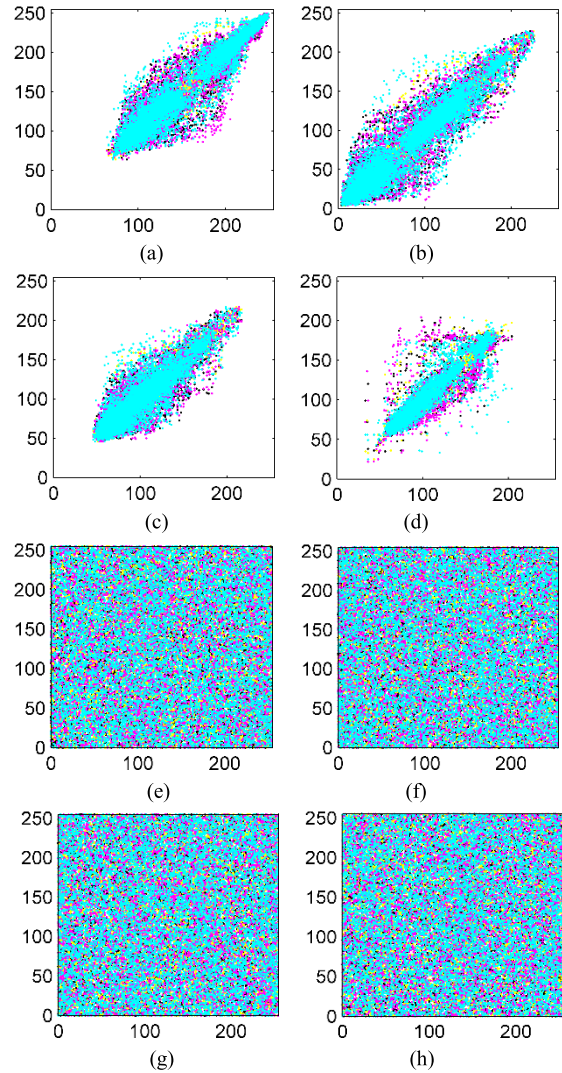


FIGURE 11. Correlation of differen image channels: (a)red channel, (b)green channel and (c)blue channel of plain image “Lena”; (d) plain grayscale image of “Cameraman”; (e)red channel, (f)green channel and (g)blue channel of encrypted image with “Lena”; (h) encrypted grayscale image of “Cameraman”, where black dots represent the horizontal direction, yellow dots represent the vertical direction, rose-red dots represent the diagonal direction, and cyan-blue dots represent the counter-diagonal direction.

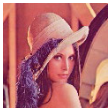







unlike the strong correlation between adjacent pixels in plain images, the correlation between adjacent pixels in encrypted images is significantly reduced and is evenly distributed.

In order to further quantitatively analyze the statistical performance of image encryption, the correlation coefficient is introduced. The correlation coefficients of adjacent pixels in the horizontal, vertical, diagonal and counter-diagonal directions are calculated using the following formula,

$$r_{x,y} = \frac{E((x - E(x))(y - E(y)))}{\sqrt{D(x) \cdot D(y)}} \quad (24)$$

where x and y are the grayscale values of two adjacent pixels, and $E(x) = 1/10000 \sum_{k=1}^{10000} x_k$, $D(x) = 1/10000 \sum_{k=1}^{10000} (x_k - E(x))^2$. From Table 4, it is evident that

TABLE 4. Correlation coefficients of different images in four directions.

		Plain image				Encrypted image			
		Horizontal	Vertical	Diagonal	Counterdiagonal	Horizontal	Vertical	Diagonal	Counterdiagonal
	Red	0.9672	0.9917	0.9601	0.9653	-5.6082×10^{-4}	4.5699×10^{-4}	-7.0556×10^{-4}	0.0011
	Green	0.9560	0.9854	0.94877	0.9467	-0.0016	0.0011	-1.3109×10^{-4}	0.0017
	Blue	0.9275	0.9691	0.9205	0.9129	3.8035×10^{-4}	3.1751×10^{-4}	-6.5770×10^{-4}	1.2089×10^{-4}
	Red	0.9395	0.9569	0.8931	0.9445	-8.1387×10^{-4}	9.7836×10^{-4}	1.3121×10^{-4}	-0.0012
	Green	0.9606	0.9761	0.9345	0.9576	-9.4454×10^{-4}	0.0012	0.0018	0.0043
	Blue	0.8950	0.9422	0.8401	0.8945	-3.0495×10^{-4}	3.4854×10^{-4}	3.0449×10^{-4}	7.6630×10^{-4}
	Red	0.9547	0.9229	0.9135	0.8751	-0.0012	0.0016	-2.7530×10^{-4}	-0.0011
	Green	0.9659	0.9580	0.9446	0.9214	-9.0577×10^{-4}	4.8925×10^{-4}	0.0014	9.2194×10^{-4}
	Blue	0.9660	0.9629	0.9505	0.9342	-7.3809×10^{-4}	2.2957×10^{-4}	-5.3466×10^{-4}	8.4728×10^{-4}
	Red	0.9817	0.9757	0.9734	0.9584	3.0103×10^{-4}	1.1301×10^{-4}	-0.0023	-4.1028×10^{-4}
	Green	0.9930	0.9884	0.9924	0.9756	-3.4782×10^{-4}	-2.3395×10^{-4}	2.8085×10^{-4}	6.4547×10^{-4}
	Blue	0.9912	0.9863	0.9903	0.9740	-0.0022	-6.7833×10^{-4}	-0.0015	-7.8598×10^{-4}
	Grayscale	0.9724	0.9797	0.9515	0.9762	-0.0012	5.0951×10^{-4}	-7.2980×10^{-4}	-2.6543×10^{-4}
	Grayscale	0.9494	0.9582	0.9014	0.9618	-3.8213×10^{-4}	0.0015	-9.1483×10^{-4}	-8.2185×10^{-4}
	Grayscale	0.9441	0.9837	0.9408	0.9378	-9.2656×10^{-4}	-0.0023	8.7946×10^{-4}	6.6901×10^{-4}
	Grayscale	0.9279	0.9558	0.9458	0.9470	-8.5767×10^{-4}	-7.5010×10^{-4}	0.0018	-9.1839×10^{-4}

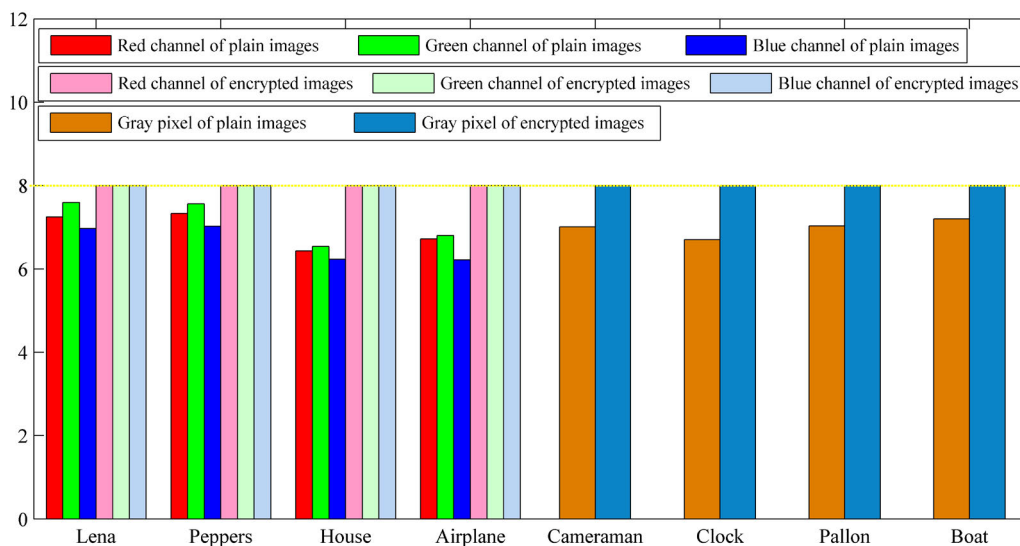


FIGURE 12. Information entropies of different encrypted images.

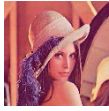







the values of correlation coefficient are mainly distributed in different directions of the plain image, which indicates that the correlation of the pixels is very high (closer to 1). While the correlations of encrypted images are uniform and are almost uncorrelated (closer to zero). Therefore, the proposed image encryption scheme can greatly reduce the correlation of the plain image.

c: INFORMATION ENTROPY ANALYSIS

Information entropy (IE) is a key parameter for calculating the randomness of encrypted images, which can be calculated as follows,

$$H(m) = \sum_{i=1}^{m \times n} P(m_i) \log_2 \left(\frac{1}{P(m_i)} \right) \quad (25)$$

TABLE 5. NPCR and UACI values of encrypted images with slight changed plain images.

		NPCR					UACI				
		(1)	(2)	(3)	(4)	(5)	(1)	(2)	(3)	(4)	(5)
	Red	99.60%	99.62%	99.66%	99.63%	99.65%	33.57%	33.64%	33.51%	33.49%	33.47%
	Green	99.64%	99.64%	99.55%	99.65%	99.61%	33.52%	33.53%	33.31%	33.39%	33.34%
	Blue	99.65%	99.57%	99.57%	99.58%	99.60%	33.32%	33.47%	33.41%	33.51%	33.40%
	Red	99.62%	99.61%	99.58%	99.59%	99.64%	33.57%	33.55%	33.32%	33.40%	33.57%
	Green	99.61%	99.61%	99.62%	99.64%	99.62%	33.51%	33.36%	33.57%	33.46%	33.40%
	Blue	99.62%	99.64%	99.63%	99.57%	99.64%	33.58%	33.42%	33.38%	33.37%	33.56%
	Red	99.63%	99.62%	99.61%	99.59%	99.63%	33.51%	33.45%	33.40%	33.59%	33.43%
	Green	99.65%	99.62%	99.65%	99.59%	99.58%	33.27%	33.48%	33.45%	33.40%	33.41%
	Blue	99.59%	99.64%	99.59%	99.60%	99.63%	33.40%	33.60%	33.48%	33.63%	33.46%
	Red	99.61%	99.62%	99.61%	99.59%	99.60%	33.56%	33.45%	33.45%	33.50%	33.46%
	Green	99.60%	99.60%	99.62%	99.59%	99.62%	33.45%	33.49%	33.42%	33.49%	33.50%
	Blue	99.62%	99.63%	99.62%	99.62%	99.61%	33.55%	33.44%	33.45%	33.47%	33.51%
	Grayscale	99.59%	99.62%	99.60%	99.62%	99.58%	33.44%	33.57%	33.39%	33.48%	33.59%
	Grayscale	99.55%	99.62%	99.62%	99.64%	99.64%	33.33%	33.50%	33.46%	33.25%	33.47%
	Grayscale	99.62%	99.63%	99.59%	99.63%	99.66%	33.37%	33.50%	33.54%	33.52%	33.51%
	Grayscale	99.64%	99.60%	99.62%	99.61%	99.63%	33.45%	33.49%	33.48%	33.40%	33.49%

where $P(m_i)$ stands for the probability of pixel grayscale value m_i , and $0 \leq P(m_i) \leq 1, \sum_{i=1}^{m \times n} P(m_i) = 1$. Assuming that the probability of pixel grayscale values 0-255 is equal, the ideal value of information entropy for randomly selected image is 8. Eight typical images are still selected for analysis, and the experimental results are shown in Fig. 12, indicating that all encrypted images can provide nearly ideal information entropy performance.

From the above analysis, it further confirms that the proposed multiagent image encryption/decryption scheme has a strong ability to resist the statistical attacks.

4) RESISTANCE TO DIFFERENTIAL ATTACKS

Due to the introduction of the concept of internal encryption keys, which means that the image encryption effect is related to the original plain image, NPCR and UACI indicators are used to analyze the impact of encryption effect. Minor modifications are made to the pixel values of the plain image, such as subtracting 1 and then taking the absolute value, selecting the positions of the modified pixels as (1) top-left corner, (2) top-right corner, (3) bottom-left corner, (4) bottom-right corner and (5) middle position. The corresponding results of 8 standard testing images are listed in Table 5. From the table, it can be observed that the NPCR of each encrypted image is close to 100%, and the UACI also approaches to the ideal value. Therefore, the proposed multiagent system

image encryption scheme can effectively resist differential attacks, as even if the original plain image undergoes slight changes, the generated encrypted image will be completely different.

VI. CONCLUSION

This paper has investigated the bipartite consensus problem for T-S fuzzy multilayer cooperation-competition multiagent networks with additive couplings and its application. Fuzzy control laws are proposed by using the output measurements from neighboring agents. Under the assumptions of the multilayer signed graphs that are undirected and simultaneously structurally balanced, sufficient conditions of bipartite consensus have been obtained for the considered multilayer multiagent networks. Coupled chaotic Lorenz systems over multilayer and signed networks have been provided to verify the validity of the derived results. Then, the obtained results are applied to image encryption/decryption by constructing a multilayer multiagent image communication system. The experimental results show that the system has excellent performance in resisting exhaustive attacks, statistical attacks and differential attacks. It could be very interesting to extend the developed results to interval type-2 T-S fuzzy Markov jump multiagent systems, which will be our research topic in near future.

REFERENCES

- [1] D. Liu, H. Liu, K. Liu, H. Gu, and J. Lü, "Robust hierarchical pinning control for nonlinear heterogeneous multiagent system with uncertainties and disturbances," *IEEE Trans. Circuits Syst. I, Reg. Papers*, vol. 69, no. 12, pp. 5273–5285, Dec. 2022, doi: [10.1109/TCSI.2022.3205364](https://doi.org/10.1109/TCSI.2022.3205364).
- [2] P. Zhao, C. Dou, K. Ma, Z. Zhang, and B. Zhang, "Distributed cooperative control based on multiagent system for islanded microgrids with switching topology and channel interruption," *IEEE Syst. J.*, vol. 16, no. 1, pp. 362–373, Mar. 2022, doi: [10.1109/JSYST.2020.3037341](https://doi.org/10.1109/JSYST.2020.3037341).
- [3] Z.-W. Liu, H. Hou, and Y.-W. Wang, "Formation-containment control of multiple underactuated surface vessels with sampling communication via hierarchical sliding mode approach," *ISA Trans.*, vol. 124, pp. 458–467, May 2022, doi: [10.1016/j.isatra.2019.12.003](https://doi.org/10.1016/j.isatra.2019.12.003).
- [4] J. Qin, Q. Ma, Y. Shi, and L. Wang, "Recent advances in consensus of multi-agent systems: A brief survey," *IEEE Trans. Ind. Electron.*, vol. 64, no. 6, pp. 4972–4983, Jun. 2017, doi: [10.1109/TIE.2016.2636810](https://doi.org/10.1109/TIE.2016.2636810).
- [5] C. Peng, J. Zhang, and Q.-L. Han, "Consensus of multiagent systems with nonlinear dynamics using an integrated sampled-data-based event-triggered communication scheme," *IEEE Trans. Syst. Man, Cybern. Syst.*, vol. 49, no. 3, pp. 589–599, Mar. 2019, doi: [10.1109/tsmc.2018.2814572](https://doi.org/10.1109/tsmc.2018.2814572).
- [6] J. Liu, T. Yin, D. Yue, H. R. Karimi, and J. Cao, "Event-based secure leader-following consensus control for multiagent systems with multiple cyber attacks," *IEEE Trans. Cybern.*, vol. 51, no. 1, pp. 162–173, Jan. 2021, doi: [10.1109/TCYB.2020.2970556](https://doi.org/10.1109/TCYB.2020.2970556).
- [7] J. Zhang, F. Wang, and G. Wen, "Bipartite consensus for networked Euler-Lagrange systems with cooperative-competitive interactions and time delays," *IET Control Theory Appl.*, vol. 17, no. 9, pp. 1214–1226, Jun. 2023, doi: [10.1049/cth2.12451](https://doi.org/10.1049/cth2.12451).
- [8] M. E. Valcher and P. Misra, "On the consensus and bipartite consensus in high-order multi-agent dynamical systems with antagonistic interactions," *Syst. Control Lett.*, vol. 66, pp. 94–103, Apr. 2014, doi: [10.1016/j.sysconle.2014.01.006](https://doi.org/10.1016/j.sysconle.2014.01.006).
- [9] R. Sakthivel, A. Parivallal, S. Manickavalli, F. Kong, and Y. Ren, "Resilient dynamic output feedback control for bipartite consensus of multiagent systems with Markov switching topologies," *Int. J. Robust Nonlinear Control*, vol. 31, no. 12, pp. 5926–5942, Aug. 2021, doi: [10.1002/rnc.5578](https://doi.org/10.1002/rnc.5578).
- [10] G. Zhao, H. Cui, and C. Hua, "Hybrid event-triggered bipartite consensus control of multiagent systems and application to satellite formation," *IEEE Trans. Autom. Sci. Eng.*, vol. 20, no. 3, pp. 1760–1771, Jul. 2023, doi: [10.1109/TASE.2022.3185643](https://doi.org/10.1109/TASE.2022.3185643).
- [11] G. Zhao and C. Hua, "Leaderless and leader-following bipartite consensus of multiagent systems with sampled and delayed information," *IEEE Trans. Neural Netw. Learn. Syst.*, vol. 34, no. 5, pp. 2220–2233, May 2023, doi: [10.1109/TNNLS.2021.3106015](https://doi.org/10.1109/TNNLS.2021.3106015).
- [12] X. Zhang, X. Liu, F. L. Lewis, and X. Wang, "Bipartite tracking consensus of nonlinear multi-agent systems," *Phys. A, Stat. Mech. Appl.*, vol. 545, May 2020, Art. no. 123504, doi: [10.1016/j.physa.2019.123504](https://doi.org/10.1016/j.physa.2019.123504).
- [13] J. Ren, Q. Song, and G. Lu, "Event-triggered bipartite leader-following consensus of second-order nonlinear multi-agent systems under signed digraph," *J. Franklin Inst.*, vol. 356, no. 12, pp. 6591–6609, Aug. 2019, doi: [10.1016/j.jfranklin.2019.06.034](https://doi.org/10.1016/j.jfranklin.2019.06.034).
- [14] Q. Wang, W. He, L. Zino, D. Tan, and W. Zhong, "Bipartite consensus for a class of nonlinear multi-agent systems under switching topologies: A disturbance observer-based approach," *Neurocomputing*, vol. 488, pp. 130–143, Jun. 2022, doi: [10.1016/j.neucom.2022.02.081](https://doi.org/10.1016/j.neucom.2022.02.081).
- [15] Y. Wu, L. Liu, J. Hu, and G. Feng, "Adaptive antisynchronization of multilayer reaction-diffusion neural networks," *IEEE Trans. Neural Netw. Learn. Syst.*, vol. 29, no. 4, pp. 807–818, Apr. 2018, doi: [10.1109/TNNLS.2017.2647811](https://doi.org/10.1109/TNNLS.2017.2647811).
- [16] J. Chen, J. Li, and R. Duan, "T-S fuzzy model-based adaptive repetitive consensus control for second-order multi-agent systems with imprecise communication topology structure," *Neurocomputing*, vol. 331, pp. 176–188, Feb. 2019, doi: [10.1016/j.neucom.2018.11.040](https://doi.org/10.1016/j.neucom.2018.11.040).
- [17] W. He, G. Chen, Q.-L. Han, W. Du, J. Cao, and F. Qian, "Multi-agent systems on multilayer networks: Synchronization analysis and network design," *IEEE Trans. Syst. Man, Cybern. Syst.*, vol. 47, no. 7, pp. 1655–1667, Jul. 2017, doi: [10.1109/TSMC.2017.2659759](https://doi.org/10.1109/TSMC.2017.2659759).
- [18] J. Zhuang, J. Cao, L. Tang, Y. Xia, and M. Perc, "Synchronization analysis for stochastic delayed multilayer network with additive couplings," *IEEE Trans. Syst. Man, Cybern. Syst.*, vol. 50, no. 11, pp. 4807–4816, Nov. 2020, doi: [10.1109/TSMC.2018.2866704](https://doi.org/10.1109/TSMC.2018.2866704).
- [19] P. Wang, G. Wen, X. Yu, W. Yu, and T. Huang, "Synchronization of multi-layer networks: From node-to-node synchronization to complete synchronization," *IEEE Trans. Circuits Syst. I, Reg. Papers*, vol. 66, no. 3, pp. 1141–1152, Mar. 2019, doi: [10.1109/TCSI.2018.2877414](https://doi.org/10.1109/TCSI.2018.2877414).
- [20] H. Yang, Z. Wang, Q. Song, X. Liu, and M. Xiao, "Quasi-synchronization of multilayer heterogeneous networks with a dynamic leader," *Int. J. Robust Nonlinear Control*, vol. 30, no. 7, pp. 2736–2751, May 2020, doi: [10.1002/rnc.4903](https://doi.org/10.1002/rnc.4903).
- [21] D. Ning, X. Wu, J. Liu, and J. Lü, "Leader-following pinning synchronization of multiagent systems with impulsive interlayer coupling," *IEEE Trans. Circuits Syst. I, Reg. Papers*, vol. 67, no. 12, pp. 5162–5174, Dec. 2020, doi: [10.1109/TCSI.2020.3018332](https://doi.org/10.1109/TCSI.2020.3018332).
- [22] X. Zhao, J. Zhou, and J.-A. Lu, "Pinning synchronization of multiplex delayed networks with stochastic perturbations," *IEEE Trans. Cybern.*, vol. 49, no. 12, pp. 4262–4270, Dec. 2019, doi: [10.1109/TCYB.2018.2861822](https://doi.org/10.1109/TCYB.2018.2861822).
- [23] Z. Wang, X. Jin, L. Pan, Y. Feng, and J. Cao, "Quasi-synchronization of delayed stochastic multiplex networks via impulsive pinning control," *IEEE Trans. Syst. Man, Cybern. Syst.*, vol. 52, no. 9, pp. 5389–5397, Sep. 2022, doi: [10.1109/TSMC.2021.3124158](https://doi.org/10.1109/TSMC.2021.3124158).
- [24] Y. Ren, H. Jiang, C. Hu, X. Li, and X. Qin, "Fully aperiodic intermittent pinning control for exponential bipartite synchronization of multilayer signed stochastic coupled neural networks," *Neurocomputing*, vol. 546, Aug. 2023, Art. no. 126354, doi: [10.1016/j.neucom.2023.126354](https://doi.org/10.1016/j.neucom.2023.126354).
- [25] Y. Xu, T. Lin, X. Liu, and W. Li, "Exponential bipartite synchronization of fractional-order multilayer signed networks via hybrid impulsive control," *IEEE Trans. Cybern.*, vol. 53, no. 6, pp. 3926–3938, Jun. 2023, doi: [10.1109/TCYB.2022.3190413](https://doi.org/10.1109/TCYB.2022.3190413).
- [26] Y. Guo and Y. Li, "Bipartite leader-following synchronization of fractional-order delayed multilayer signed networks by adaptive and impulsive controllers," *Appl. Math. Comput.*, vol. 430, Oct. 2022, Art. no. 127243, doi: [10.1016/j.amc.2022.127243](https://doi.org/10.1016/j.amc.2022.127243).
- [27] T. Takagi and M. Sugeno, "Fuzzy identification of systems and its applications to modeling and control," *IEEE Trans. Syst. Man, Cybern.*, vol. SMC-15, no. 1, pp. 116–132, Jan. 1985.
- [28] X. Wang, J. H. Park, H. Yang, X. Zhang, and S. Zhong, "Delay-dependent fuzzy sampled-data synchronization of T-S fuzzy complex networks with multiple couplings," *IEEE Trans. Fuzzy Syst.*, vol. 28, no. 1, pp. 178–189, Jan. 2020, doi: [10.1109/TFUZZ.2019.2901353](https://doi.org/10.1109/TFUZZ.2019.2901353).
- [29] C. Huang, X. Zhang, H.-K. Lam, and S.-H. Tsai, "Synchronization analysis for nonlinear complex networks with reaction-diffusion terms using fuzzy-model-based approach," *IEEE Trans. Fuzzy Syst.*, vol. 29, no. 6, pp. 1350–1362, Jun. 2021, doi: [10.1109/TFUZZ.2020.2974143](https://doi.org/10.1109/TFUZZ.2020.2974143).
- [30] R. Sakthivel, O.-M. Kwon, M. J. Park, S.-G. Choi, and R. Sakthivel, "Robust asynchronous filtering for discrete-time T-S fuzzy complex dynamical networks against deception attacks," *IEEE Trans. Fuzzy Syst.*, vol. 30, no. 8, pp. 3257–3269, Aug. 2022, doi: [10.1109/TFUZZ.2021.3111453](https://doi.org/10.1109/TFUZZ.2021.3111453).
- [31] Y. Wu, R. Lu, P. Shi, H. Su, and Z.-G. Wu, "Sampled-data synchronization of complex networks with partial couplings and T-S fuzzy nodes," *IEEE Trans. Fuzzy Syst.*, vol. 26, no. 2, pp. 782–793, Apr. 2018, doi: [10.1109/TFUZZ.2017.2688490](https://doi.org/10.1109/TFUZZ.2017.2688490).
- [32] Z. Zhang and J. Dong, "Containment control of interval type-2 fuzzy multi-agent systems with multiple intermittent packet dropouts and actuator failure," *J. Franklin Inst.*, vol. 357, no. 10, pp. 6096–6120, Jul. 2020, doi: [10.1016/j.jfranklin.2020.04.003](https://doi.org/10.1016/j.jfranklin.2020.04.003).
- [33] Z. Wang, D. Xue, and F. Pan, "Output consensus for fuzzy singular multi-agent fractional order systems with actuator saturation," *IEEE Trans. Circuits Syst. II, Exp. Briefs*, vol. 69, no. 8, pp. 3465–3469, Aug. 2022, doi: [10.1109/TCSI.2022.3156985](https://doi.org/10.1109/TCSI.2022.3156985).
- [34] G. Narayanan, M. S. Ali, Q. Zhu, B. Priya, and G. K. Thakur, "Fuzzy observer-based consensus tracking control for fractional-order multi-agent systems under cyber-attacks and its application to electronic circuits," *IEEE Trans. Netw. Sci. Eng.*, vol. 10, no. 2, pp. 698–708, Mar. 2023, doi: [10.1109/TNSE.2022.3217618](https://doi.org/10.1109/TNSE.2022.3217618).
- [35] S. Yang, W. Zhang, D. Ruan, T. Yang, and Y. Li, "Fast fixed-time impulsive bipartite synchronization of TS fuzzy complex networks with signed graphs," *Nonlinear Anal., Hybrid Syst.*, vol. 48, May 2023, Art. no. 101325, doi: [10.1016/j.nahs.2022.101325](https://doi.org/10.1016/j.nahs.2022.101325).
- [36] R. Sakthivel, A. Parivallal, F. Kong, and Y. Ren, "Bipartite consensus for Takagi-Sugeno fuzzy uncertain multi-agent systems with gain fluctuations," *IEEE Trans. Signal Inf. Process. over Netw.*, vol. 9, pp. 74–83, Feb. 2023, doi: [10.1109/TSIPN.2023.3239679](https://doi.org/10.1109/TSIPN.2023.3239679).

- [37] Y. Feng, K. Dai, and X. Chen, "Enhanced distributed consensus filtering over lossy wireless sensor networks with application to target speed tracking," *IEEE Trans. Ind. Electron.*, vol. 70, no. 9, pp. 9368–9378, Sep. 2023, doi: [10.1109/TIE.2022.3208578](https://doi.org/10.1109/TIE.2022.3208578).
- [38] J. G. Romero, E. Nuño, and C. I. Aldana, "Robust PID consensus-based formation control of nonholonomic mobile robots affected by disturbances," *Int. J. Control*, vol. 96, no. 3, pp. 791–799, Mar. 2023, doi: [10.1080/00207179.2021.2015541](https://doi.org/10.1080/00207179.2021.2015541).
- [39] S. Mo, W.-H. Chen, and X. Lu, "Hierarchical hybrid control for scaled consensus and its application to secondary control for DC microgrid," *IEEE Trans. Cybern.*, vol. 53, no. 7, pp. 4446–4458, Jul. 2023, doi: [10.1109/TCYB.2022.3182036](https://doi.org/10.1109/TCYB.2022.3182036).
- [40] T. Wu, S. Gorbachev, H.-K. Lam, J. H. Park, L. Xiong, and J. Cao, "Adaptive event-triggered space-time sampled-data synchronization for fuzzy coupled RDNNs under hybrid random cyberattacks," *IEEE Trans. Fuzzy Syst.*, vol. 31, no. 6, pp. 1855–1869, Jun. 2023, doi: [10.1109/TFUZZ.2022.3215747](https://doi.org/10.1109/TFUZZ.2022.3215747).
- [41] M. Bernal, A. Sala, Z. Lendek, and T. M. Guerra, "Takagi–Sugeno models," in *Analysis and Synthesis of Nonlinear Control Systems: A Convex Optimisation Approach*. Berlin, Germany: Springer, 2022, pp. 24–27.
- [42] J. Ren, Q. Song, Y. Gao, M. Zhao, and G. Lu, "Leader-following consensus of delayed neural networks under multi-layer signed graphs," *Neurocomputing*, vol. 450, pp. 168–182, Aug. 2021, doi: [10.1016/j.neucom.2021.03.009](https://doi.org/10.1016/j.neucom.2021.03.009).
- [43] J. Hu, Y. Wu, L. Liu, and G. Feng, "Adaptive bipartite consensus control of high-order multiagent systems on cooperation networks," *Int. J. Robust Nonlinear Control*, vol. 28, no. 7, pp. 2868–2886, May 2018, doi: [10.1002/rnc.4054](https://doi.org/10.1002/rnc.4054).
- [44] J. Hu, Y. Wu, T. Li, and B. K. Ghosh, "Consensus control of general linear multiagent systems with antagonistic interactions and communication noises," *IEEE Trans. Autom. Control*, vol. 64, no. 5, pp. 2122–2127, May 2019, doi: [10.1109/TAC.2018.2872197](https://doi.org/10.1109/TAC.2018.2872197).
- [45] E. Nuño, A. Loria, E. Panteley, and E. Restrepo, "Rendezvous of nonholonomic robots via output-feedback control under time-varying delays," *IEEE Trans. Control Syst. Technol.*, vol. 30, no. 6, pp. 2707–2716, Nov. 2022, doi: [10.1109/TCST.2022.3144031](https://doi.org/10.1109/TCST.2022.3144031).
- [46] G. Wang, "Consensus algorithm for multiagent systems with nonuniform communication delays and its application to nonholonomic robot rendezvous," *IEEE Trans. Control Netw. Syst.*, vol. 10, no. 3, pp. 1496–1507, Sep. 2023, doi: [10.1109/TCNS.2022.3233101](https://doi.org/10.1109/TCNS.2022.3233101).
- [47] T. Taniguchi, K. Tanaka, H. Ohtake, and H. O. Wang, "Model construction, rule reduction, and robust compensation for generalized form of Takagi–Sugeno fuzzy systems," *IEEE Trans. Fuzzy Syst.*, vol. 9, no. 4, pp. 525–538, Aug. 2001, doi: [10.1109/91.940966](https://doi.org/10.1109/91.940966).



XINHUA WU received the B.S. degree in electronic and information engineering from Nantong University, in 2003, and the M.S. degree in electronics and communication engineering from Shanghai University, in 2010. He has been with the School of Information Engineering, Jiangsu College of Engineering and Technology, since 2007, where he is currently a Senior Engineer. His current research interests include the distributed control of multiagent systems and bipartite consensus control.



SUYING SHENG received the B.E. degree in electrical engineering and automation from Nantong University, Nantong, in 2003, the M.S. degree in communication and information system from Soochow University, Suzhou, in 2006, and the Ph.D. degree in information and communication engineering from Nantong University, in 2020. She has been with the School of Electrical Engineering, Nantong University, since 2006, where she is currently a Senior Experimentalist. Her current research interests include distributed estimation over sensor networks, dynamical networks complex, multiagent systems, and fuzzy systems.



GUOPING LU received the B.S. degree from the Department of Applied Mathematics, Chengdu University of Science and Technology, China, in 1984, and the M.S. and Ph.D. degrees from the Department of Mathematics, East China Normal University, China, in 1989 and 1998, respectively. He is currently a Professor with the School of Electrical Engineering, Nantong University, Jiangsu, China. His current research interests include singular systems, multiagent systems, networked control, and nonlinear signal processing.

• • •